

Origin of the orbital architecture of the giant planets of the Solar System

K. Tsiganis¹, R. Gomes^{1,2}, A. Morbidelli¹ & H. F. Levison^{1,3}

Planetary formation theories^{1,2} suggest that the giant planets formed on circular and coplanar orbits. The eccentricities of Jupiter, Saturn and Uranus, however, reach values of 6 per cent, 9 per cent and 8 per cent, respectively. In addition, the inclinations of the orbital planes of Saturn, Uranus and Neptune take maximum values of ~ 2 degrees with respect to the mean orbital plane of Jupiter. Existing models for the excitation of the eccentricity of extrasolar giant planets^{3–5} have not been successfully applied to the Solar System. Here we show that a planetary system with initial quasi-circular, coplanar orbits would have evolved to the current orbital configuration, provided that Jupiter and Saturn crossed their 1:2 orbital resonance. We show that this resonance crossing could have occurred as the giant planets migrated owing to their interaction with a disk of planetesimals^{6,7}. Our model reproduces all the important characteristics of the giant planets' orbits, namely their final semimajor axes, eccentricities and mutual inclinations.

The planetary migration discussed above is a natural result of planet formation. After the giant planets were formed and the circumsolar gaseous nebula was dissipated, the Solar System was composed of the Sun, the planets and a debris disk of small

planetesimals. The planets then started to erode the disk, by either accreting or scattering away the planetesimals. The planets migrated because of the exchange of angular momentum with the disk particles during this process^{6,7}. Numerical simulations⁸ show that Jupiter was forced to move inward, while Saturn, Uranus and Neptune drifted outward. The orbital distribution of trans-neptunian objects is probably the result of such planetary migration⁷, and suggests that Neptune probably started migrating well inside 20 AU while the disk was extended up to 30–35 AU (refs 9–11).

During migration, the eccentricities and mutual inclinations of the planets are damped because of their gravitational interaction with the disk particles, in a process known as dynamical friction¹². However, the planets' orbital periods also change. If initially the planets' orbits were sufficiently close to each other, it is likely that they had to pass through low-order mean motion resonances (MMRs), which occur when the ratio between two orbital periods is equal to a ratio of small integers. These resonance crossings could have excited the orbital eccentricities of the resonance crossing planets. We focus our investigation on the 1:2 MMR between Jupiter and Saturn, as it is the strongest resonance.

In all our simulations, we started with a system where the initial

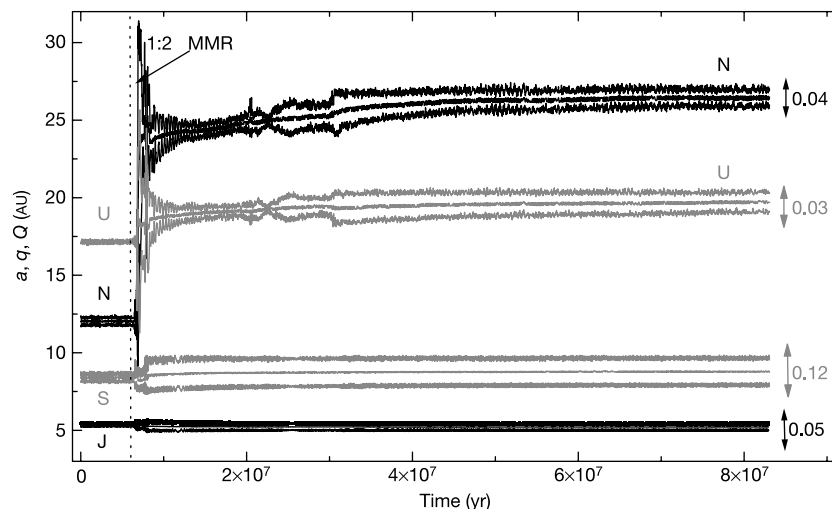


Figure 1 | Orbital evolution of the giant planets. These are taken from a N -body simulation with $35M_E$ 'hot' disk composed of 3,500 particles and truncated at 30 AU. Three curves are plotted for each planet: the semimajor axis (a) and the minimum (q) and maximum (Q) heliocentric distances. U, Uranus; N, Neptune; S, Saturn; J, Jupiter. The separation between the upper and lower curves for each planet is indicative of the eccentricity of the orbit. The maximum eccentricity of each orbit, computed over the last 2 Myr of

evolution, is noted on the plot. The vertical dotted line marks the epoch of 1:2 MMR crossing. After this point, curves belonging to different planets begin to cross, which means that the planets encounter each other. During this phase, the eccentricities of Uranus and Neptune can exceed 0.5. In this run, the two ice giants exchange orbits. This occurred in $\sim 50\%$ of our simulations.

¹Observatoire de la Côte d'Azur, CNRS, BP 4229, 06304 Nice Cedex 4, France. ²GEA/OV/UFRJ and ON/MCT, Ladeira do Pedro Antonio, 43-Centro 20.080-090, Rio de Janeiro, RJ, Brazil. ³Department of Space Studies, Southwest Research Institute, 1050 Walnut Street, Suite 400, Boulder, Colorado 80302, USA.

semimajor axis, a , of Jupiter was set to $a_J = 5.45$ AU and Saturn was placed a few tenths of an AU interior to the 1:2 MMR ($a_{1:2} \approx 8.65$ AU). The initial semimajor axes of the ice giants (Uranus and Neptune) were varied in the ranges 11–13 AU and 13.5–17 AU, while keeping their initial orbital separation larger than 2 AU. In all cases, the initial orbits of all the giant planets were nearly circular and coplanar (eccentricities, e , and mutual inclinations, i , $\sim 10^{-3}$). In addition to the giant planets, our simulations included a massive $((30\text{--}50)M_E$, where M_E is the mass of the Earth) particle disk, consisting of 1,000–5,000 equal-mass bodies, starting just beyond the orbits of the planets, ending between 30 and 35 AU, and with a surface density that falls linearly with heliocentric distance. It has been shown that, although this resolution is not enough to model all aspects of planetary migration¹¹, it adequately models the macroscopic evolution of the planetary orbits. Both dynamically ‘cold’ ($e \approx \sin i \approx 10^{-3}$) and dynamically ‘hot’ ($e \approx \sin i \approx 0.05$) disks were considered. We simulated the dynamical evolution of 43 different systems, using two different N -body codes, SyMBA¹³ and MERCURY¹⁴, with a time step of 0.25–0.5 years. In these experiments the self-gravity of the disk was ignored.

A typical example of the evolution undergone by our systems is shown in Fig. 1. At 6.6 Myr, after a period of slow migration on nearly circular orbits, Jupiter and Saturn cross the 1:2 MMR, at which point their eccentricities are quickly excited to values comparable to the ones currently observed. These ‘kicks’ in eccentricity are the result of the planets jumping over the 1:2 MMR without being trapped, and are qualitatively predicted by adiabatic theory (see Supplementary Information).

The sudden jump in the eccentricities of Jupiter and Saturn described above has a drastic effect on the planetary system as a whole, as shown in Fig. 1. The secular perturbations that Jupiter and Saturn exert on Uranus and Neptune force the eccentricities of the ice giants to increase by an amount that depends on the masses and semimajor axes of all planets¹⁵. As a result of the ‘compactness’ of the system, the planetary orbits become chaotic and intersect. When this occurs, a short phase of encounters follows the resonance crossing event. These encounters increase the inclinations of the planetary orbits by $1^\circ\text{--}7^\circ$. In addition, both ice giants are scattered outward and penetrate the disk. Thus, the flux of small bodies towards Saturn and Jupiter, and hence their rate of migration, increases abruptly. During this fast migration phase, the eccentricities and inclinations of the planets slowly decrease by dynamical friction and the planetary system is stabilized. The planets stop migrating when the disk is almost completely depleted. As shown in Fig. 1, not only their final semimajor axes, but also their final eccentricities, are close to the observed values.

The final orbits of the planets depend on the evolution of the system immediately after the resonance crossing event. Although there were many free parameters in our initial conditions, we found that the final configuration is most sensitive to the initial orbital separation between the ice giants ($\Delta a_{1,2}$) and, more importantly, to the one between Saturn and the inner ice giant ($\Delta a_{S,I_1}$). In our simulations, $\Delta a_{1,2}$ ranged from ~ 2 to ~ 6 AU, while $\Delta a_{S,I_1}$ ranged from ~ 2.5 to ~ 5 AU.

For $\Delta a_{S,I_1} < 3$ AU, the probability that Saturn scatters one of the ice giants to a Jupiter-crossing orbit increases. In such cases, the ice giant is ejected from the system. This happened in 14 (33%) of our runs. All other runs (67%) were successfully completed, that is, all four planets eventually reached stable orbits. Only two cases were found in which no encounters between the giant planets occurred. They both had $\Delta a_{S,I_1} \approx 5$ AU, which means that they were among the least compact systems that we simulated. In these runs, the semimajor axis of Uranus barely reached 16 AU, as in ref. 11. Repeated encounters between the ice giants were seen in all other successful runs. In 13 of them, only the ice giants encountered one another ($\Delta a_{S,I_1} \geq 3.5$ AU). For $\Delta a_{S,I_1} < 3.5$ AU, encounters between Saturn and an ice giant also occurred. Encounters with Saturn affect the dynamics of the

Jupiter–Saturn subsystem, allowing the gas giants to maintain their eccentricities against dynamical friction. This type of evolution was observed in 14 of our runs (33%). We note that, in this type of evolution, the duration of the fast migration phase is shorter than in the other cases.

Although we have not thoroughly explored the available parameter space, our experiments enable us to evaluate statistically the proposed excitation mechanism. We distinguish between two classes of runs: first, those in which there were no encounters between an ice giant and a gas giant (class A, 15 runs), and second, those in which Saturn suffered an encounter with one or both ice giants (class B, 14 runs). For each class, we computed the mean and standard deviation of the semimajor axis, proper eccentricity and proper inclination of each planet. Figure 2 shows the comparison between these quantities and the proper orbital elements of the real giant planets. Both classes of runs produce satisfactory results. Planetary orbits with very high eccentricities or inclinations are not produced. However, it is clear from this figure that class B runs ($\sim 50\%$ of our successful runs) give a much better match of the outer Solar System. In fact, the three orbital elements of all the real giant planets have values that lie within one standard deviation from the mean values of class B runs.

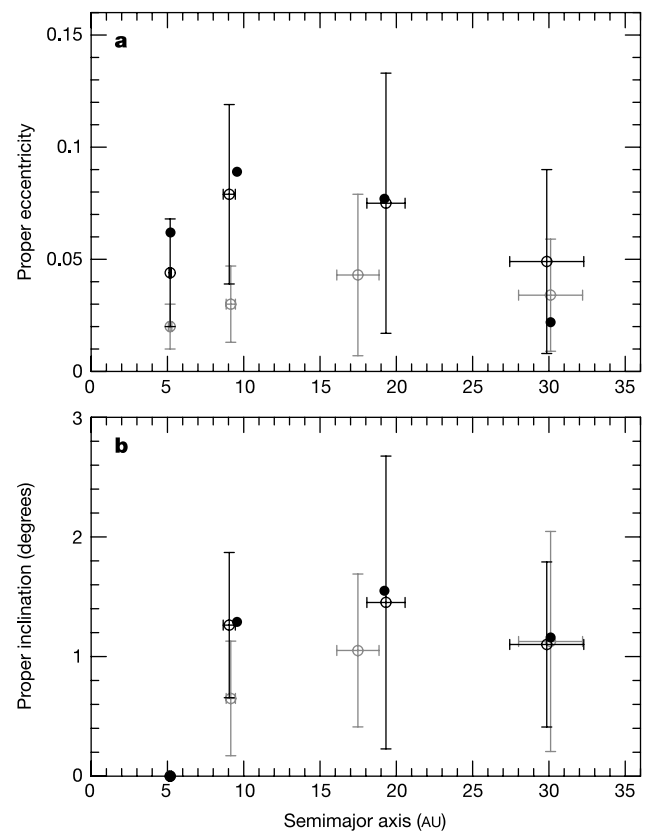


Figure 2 | Comparison of our synthetic final planetary systems with the outer Solar System. **a**, Proper eccentricity versus semimajor axis. **b**, Proper inclination versus semimajor axis. Proper eccentricities and inclinations are defined as the maximum values acquired over a 2-Myr timespan and were computed from numerical integrations. The inclinations are measured relative to Jupiter’s orbital plane. These values for the real planets are presented with filled black circles. The open grey circles mark the mean of the proper values for the runs of class A (no encounters for Saturn), while the open black circles mark the same quantities for the runs of class B (see text for the definition of these classes). The error bars represent one standard deviation. The largest values of the proper eccentricity and inclination of our synthetic planets were $e = 0.11$ for Jupiter, $e = 0.17$ and $i = 2.5^\circ$ for Saturn, $e = 0.23$ and $i = 4.5^\circ$ for Uranus, and $e = 0.17$ and $i = 4.0^\circ$ for Neptune.

The final semimajor axes of the planets are an important diagnostic of migration models. The simulations of compact systems in ref. 11 always produced final configurations in which Neptune was at ~ 30 AU, but Uranus was too close to the Sun. Our model nicely solves this nagging problem. As shown in Fig. 2, class B runs give $a_U = 19.3 \pm 1.3$ AU and $a_N = 29.9 \pm 2.4$ AU, the observed values being $a_U = 19.2$ AU and $a_N = 30.1$ AU. (Here a_U and a_N are the semimajor axes of Uranus and Neptune, respectively.) The final orbital separation of Jupiter and Saturn depends on the amount of mass that they process during the evolution of the system — that is, on the initial mass of the disk. Although larger disk masses favour the stability of the four-planet system, we found that, for disk masses larger than $\sim (35\text{--}40)M_E$, the final orbital separation of Jupiter and Saturn tends to be larger than is actually observed. For disks of $50M_E$, Saturn was found to cross the 2:5 MMR with Jupiter. In addition, the final eccentricities of the two planets were too small, because they had experienced too much dynamical friction. Indeed, the fact that we reproduce both the semimajor axes and the eccentricities/inclinations in the same integrations is a strong point of our model.

The initial dynamical state of the disk also affects the final state of the planetary system. ‘Hot’ disks tend to produce systems where the eccentricities for Jupiter and Saturn are larger than in ‘cold’ disks. The actual disk may indeed have been as excited as we assumed in our ‘hot’ runs, because of the presence of a large number of Pluto-sized objects¹⁶.

Other compact planetary configurations could lead to the crossing of different MMRs. For reasons of completeness, we studied the crossing of the 2:3 and 1:2 MMRs between (1) Saturn and the inner ice giant, and (2) the two ice giants, by placing Saturn exterior to the 1:2 MMR with Jupiter, and varying the initial positions of Uranus and Neptune. We found that, although some of these resonance crossings may destabilize the orbits of the ice giants, none can excite the orbit of Jupiter.

The survivability of the regular satellites during the planetary encounters is a potential issue with our model. Thus, during eight migration simulations we recorded all encounters deeper than one Hill radius (approximately the distance within which the gravity of the planet dominates over the gravity of the Sun). We then integrated the evolution of the regular satellites of Saturn and the ice giants during a re-enactment of these encounters. We assumed that both ice giants had Uranus’s satellite system. We found that in half of the simulations, all of the satellite systems survived the entire suite of encounters (that is, $\sin i, e < 0.05$). Thus, we conclude that the survivability of the satellites is not a problem for the model. However, we note that the irregular satellites would not survive the encounters. Thus, if this model is correct they must have been captured either during or after the 1:2 MMR crossing.

We noticed in our simulations that several particles were trapped on long-lived orbits characteristic of Neptune’s Trojan asteroids (two per run, on average, with a lifetime larger than 80 Myr). Their eccentricities reached values < 0.1 . These particles were eventually removed from the Trojan region, but this is probably an artefact of the graininess of Neptune’s migration⁸ (although this graininess could also have been responsible for their capture). Jupiter’s Trojans are a more subtle issue, described in ref. 17, which also turns out to be a strength of our model.

Thus we conclude that the eccentricities of Jupiter and Saturn are

probably the result of the fact that these planets crossed the 1:2 MMR. Other mechanisms^{3–5} that have been proposed for the eccentricity excitation of extrasolar planets have neither been applied to our Solar System nor confronted with the large body of constraints that its current structure provides. Our model statistically reproduces all aspects of the orbits of the giant planets. It is consistent with the existence of regular satellites, with the observed distributions of Jupiter’s Trojans¹⁷, perhaps with the existence of Neptune’s Trojans, and does not contradict the distribution of main-belt asteroids¹⁸.

Received 6 December 2004; accepted 11 March 2005.

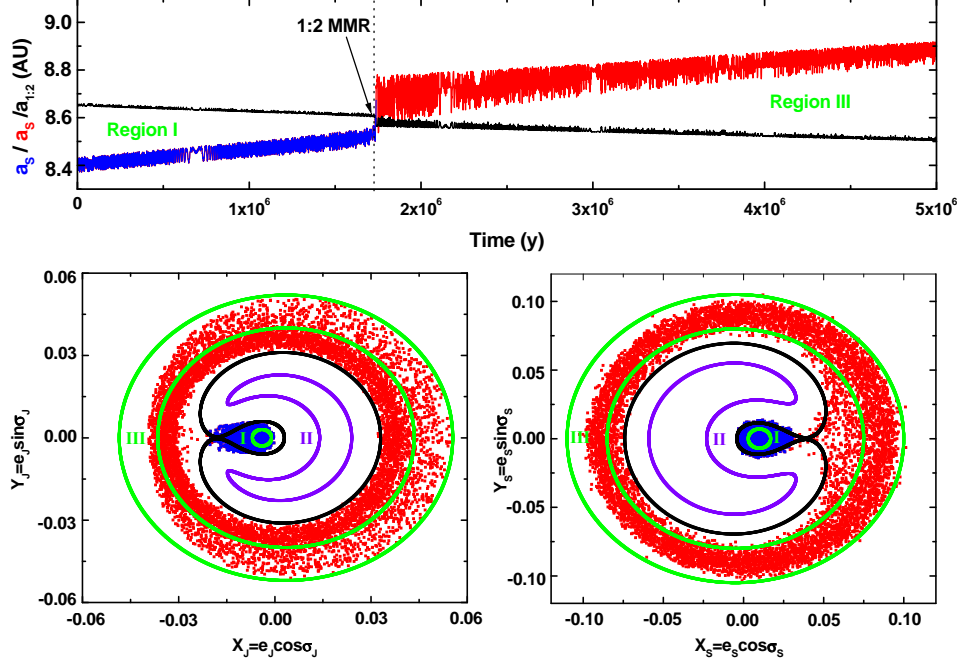
- Pollack, J. B. *et al.* Formation of the giant planets by concurrent accretion of solids and gas. *Icarus* **164**, 62–85 (1996).
- Lubow, S. H., Seibert, M. & Artymowicz, P. Disk accretion onto high-mass planets. *Astrophys. J.* **526**, 1001–1012 (1999).
- Goldreich, P. & Sari, R. Eccentricity evolution for planets in gaseous disks. *Astrophys. J.* **585**, 1024–1037 (2003).
- Papaloizou, J. C. B., Nelson, R. P. & Masset, F. Orbital eccentricity growth through disk-companion tidal interaction. *Astron. Astrophys.* **366**, 263–275 (2001).
- Zakamska, N. L. & Tremaine, S. Excitation and propagation of eccentricity disturbances in planetary systems. *Astron. J.* **128**, 869–877 (2004).
- Fernandez, J. A. & Ip, W.-H. Some dynamical aspects of the accretion of Uranus and Neptune—The exchange of orbital angular momentum with planetesimals. *Icarus* **58**, 109–120 (1984).
- Malhotra, R. The origin of Pluto’s orbit: implications for the Solar System beyond Neptune. *Astron. J.* **110**, 420–432 (1995).
- Hahn, J. M. & Malhotra, R. Orbital evolution of planets embedded in a planetesimal disk. *Astron. J.* **117**, 3041–3053 (1999).
- Gomes, R. The origin of the Kuiper Belt high-inclination population. *Icarus* **161**, 404–418 (2003).
- Levison, H. F. & Morbidelli, A. The formation of the Kuiper belt by the outward transport of bodies during Neptune’s migration. *Nature* **426**, 419–421 (2003).
- Gomes, R. S., Morbidelli, A. & Levison, H. F. Planetary migration in a planetesimal disk: Why did Neptune stop at 30 AU? *Icarus* **170**, 492–507 (2004).
- Kokubo, E. & Ida, S. Orbital evolution of protoplanets embedded in a swarm of planetesimals. *Icarus* **114**, 247–257 (1995).
- Duncan, M. J., Levison, H. F. & Lee, M. H. A multiple time step symplectic algorithm for integrating close encounters. *Astron. J.* **116**, 2067–2077 (1998).
- Chambers, J. E. A hybrid symplectic integrator that permits close encounters between massive bodies. *Mon. Not. R. Astron. Soc.* **304**, 793–799 (1999).
- Murray, C. & Dermott, S. F. *Solar System Dynamics* (Cambridge Univ. Press, Cambridge, UK, 1999).
- Stern, S. A. On the number of planets in the outer solar system—Evidence of a substantial population of 1000-km bodies. *Icarus* **90**, 271–281 (1991).
- Morbidelli, A., Levison, H. F., Tsiganis, K. & Gomes, R. Chaotic capture of Jupiter’s Trojan asteroids in the early Solar System. *Nature* doi:10.1038/nature03540 (this issue).
- Gomes, R., Tsiganis, K., Morbidelli, A. & Levison, H. F. Origin of the cataclysmic Late Heavy Bombardment period of the terrestrial planets. *Nature* doi:10.1038/nature03676 (this issue).

Supplementary Information is linked to the online version of the paper at www.nature.com/nature.

Acknowledgements R.G. is grateful to the Conselho Nacional de Desenvolvimento Científico e Tecnológico for financial support of his sabbatical year in the OCA observatory in Nice. The work of K.T. was supported by an EC Marie Curie Individual Fellowship. A.M. and H.F.L. thank the CNRS and the NSF for funding the collaboration between the OCA and the SwRI groups. H.F.L. is grateful to NASA’s Origins and PG&G programmes.

Author Information Reprints and permissions information is available at npg.nature.com/reprintsandpermissions. The authors declare no competing financial interests. Correspondence and requests for materials should be addressed to A.M. (morby@obs-nice.fr).

Supplemental Material



A Detailed illustration of the 1:2 MMR crossing of Jupiter and Saturn.

The top panel shows the semi-major axis of Saturn (blue/red curve) and the exact location of the 1:2 MMR with Jupiter (black curve) as functions of time. The dotted vertical line marks the time of resonance crossing at $t = 1.72$ My.

The bottom panels show the dynamical structure of the 1:2 resonance for Jupiter (left) and Saturn (right) respectively. The natural way to represent the resonance dynamics is with polar coordinates, with the eccentricity e as the radius and the so-called critical argument of the resonance σ as the angle. In this case, the critical argument of the resonance felt by Jupiter is $\sigma_J = \lambda_J - 2\lambda_S + \varpi_J$ while that of the resonance felt by Saturn is $\sigma_S = \lambda_J - 2\lambda_S + \varpi_S$, where λ and ϖ are the mean longitude and the longitude of perihelion, respectively, and the index J/S refers to Jupiter/Saturn (see chapter 9 of [S1]). The curves in the bottom panels are free hand illustrations of the dynamics near and inside the resonance. The green

curves represent orbits in the non-resonant regions. There are two of such regions. Region I, at small eccentricity, is called the region of ‘apocentric libration’ or ‘inner circulation’, while Region III, at large eccentricity ($e \gtrsim 0.05$), is called the region of ‘external circulation’. The banana-shaped violet curves represent orbits in the resonant Region II. Along these orbits the critical angle σ librates. The border between all three regions is the black self-crossing curve, called the ‘separatrix’. Regions I and III only touch each other at the crossing point (or **X** point) of the separatrix, which is an unstable equilibrium point of the dynamics.

As the planets approach exact resonance during migration, the **X** point moves toward smaller eccentricities, i.e. Region I shrinks and Region III grows. Adiabatic theory [S2-S4] predicts that Jupiter and Saturn should continue to evolve in Region I (blue dots in the bottom panels, which correspond to the temporal evolution in the top panel before $t = 1.72$ My), until Region I shrinks so much that its area becomes smaller than that filled by the planets’ evolution. When this occurs, the **X** point touches the region inhabited by the planet. The curves drawn in the bottom panels are intended to represent a snapshot of the dynamics at this exact instant. At this time, the planets must jump from Region I to Region III (red dots), by passing through the ‘X’ point. This, in turn, causes a jump in eccentricity. Because of the conservation of the actions $2\sqrt{a_J} - \sqrt{a_J(1 - e_J^2)}$ and $\sqrt{a_S} - 2\sqrt{a_S(1 - e_S^2)}$, the jumps of the eccentricities are correlated with a jump of the semi-major axes a_J, a_S . The jump of a_S is visible in the top panel at the transition from the blue to the red color.

The amplitude of the eccentricity jump can be quantitatively predicted from the shape of the separatrix curve at the moment of resonance crossing, and is a function of the planetary masses. Thus, the eccentricity excitation mechanism advocated in the main text is a deterministic one, which explains why all our simulations gave similar results (the differences being due to the evolution after the resonance

crossing, which depends on the interactions of Jupiter and Saturn with the ice giants and the disk particles). We emphasize that this resonance jumping occurs because the planets migrate in divergent directions. If the two planets were approaching each other, adiabatic theory predicts that they could be trapped in resonance (i.e. enter into Region II) (see [S5] for an example).

To illustrate the resonance crossing dynamics in detail and avoid additional ‘noise’, the simulation presented here is not one of the simulations presented in the main text. It has been performed by integrating the equations of motion of the Sun-Jupiter-Saturn system alone (no disk, no ice giants), with an additional drag force acting on the planets, using a now standard technique [S5]. The drag force was designed so to force the two planets to migrate at the same rate as seen in our N -body simulations.

References:

- [S1] Morbidelli, *Modern Celestial Mechanics: aspects of Solar System dynamics*, in “Advances in Astronomy and Astrophysics”, Taylor & Francis. (2002).
- [S2] Henrard, J. Capture into resonance - an extension of the use of adiabatic invariants. *Celestial Mechanics* 27, 3-22. (1982).
- [S3] Henrard, J., Lemaitre, A. A mechanism of formation for the Kirkwood gaps. *Icarus* 55, 482-494. (1983).
- [S4] Neishtadt, A. I. Changes in the adiabatic invariant due to separatrix crossing in systems with two degrees of freedom. *Prikladnaia Matematika i Mekhanika* 51, 750-757. (1987).
- [S5] Malhotra, R. The origin of Pluto’s orbit: implications for the Solar System beyond Neptune. *Astron. J.* 110, 420-432. (1995).

LETTERS

Chaotic capture of Jupiter's Trojan asteroids in the early Solar System

A. Morbidelli¹, H. F. Levison^{1,2}, K. Tsiganis¹ & R. Gomes^{1,3}

Jupiter's Trojans are asteroids that follow essentially the same orbit as Jupiter, but lead or trail the planet by an angular distance of ~ 60 degrees (co-orbital motion). They are hypothesized to be planetesimals that formed near Jupiter and were captured onto their current orbits while Jupiter was growing^{1,2}, possibly with the help of gas drag³⁻⁶ and/or collisions⁷. This idea, however, cannot explain some basic properties of the Trojan population, in particular its broad orbital inclination distribution, which ranges up to ~ 40 degrees (ref. 8). Here we show that the Trojans could have formed in more distant regions and been subsequently captured into co-orbital motion with Jupiter during the time when the giant planets migrated by removing neighbouring planetesimals⁹⁻¹². The capture was possible during a short period of time, just after Jupiter and Saturn crossed their mutual 1:2 resonance, when the dynamics of the Trojan region were completely chaotic. Our simulations of this process satisfactorily reproduce the orbital distribution of the Trojans and their total mass.

Recent numerical experiments^{13,14} have shown that the orbits of the giant planets are best reproduced if Saturn and Jupiter crossed their mutual 1:2 mean motion resonance (MMR) during their migration. This occurs when the ratio of their orbital periods, P_S/P_J , equals 2. The current ratio of P_S/P_J is slightly less than 2.5. However, there is a serious argument in the literature against the idea that Jupiter and Saturn crossed the 1:2 MMR. If the crossing had happened, any pre-existing jovian Trojans would have become violently unstable, and Jupiter's co-orbital region would have emptied^{15,16}. Indeed, we performed a simulation similar to that in ref. 15, but with 1.3 million particles in the Trojan region—none survived the 1:2 MMR crossing.

However, the dynamical evolution of a gravitating system of objects is time reversible. Thus, if the local objects can escape the Trojan region when the latter becomes unstable, other bodies can enter the same region and be temporarily trapped. Consequently, a transient Trojan population can be created if there is an external source of objects. In this case, the source is constituted by the very bodies that are forcing the planets to migrate⁹⁻¹², and is of considerable magnitude given how much the planets must move. When Jupiter and Saturn get far enough from the 1:2 MMR that the co-orbital region becomes stable, the population that happens to be there at that time remains trapped. It becomes the population of permanent jovian Trojans still observable today.

To investigate the above idea, we first performed a numerical simulation that involved integrating the orbits of a series of massless planetesimals initially on Saturn-crossing orbits under the gravitational influence of the Sun, Jupiter and Saturn. In this simulation, the planets were on non-migrating orbits close to the 1:2 MMR, so that the Trojan region was fully unstable. We found that $\sim 1\%$ of the planetesimals initially on Saturn-crossing orbits spent more than

100 yr as jovian Trojans, which we define as objects having orbital periods relative to Jupiter's of between 0.97 and 1.03, absolute values of angular distance from the planet of between 40° and 90° , and eccentricities of less than 0.15. These values were derived from the current orbital distribution of the Trojans. The particles temporarily trapped in the Trojan region covered the whole region of co-orbital motion. More importantly, their orbital inclination covered all values up to $\sim 40^\circ$, as a result of previous close encounters with the planets. Therefore, our idea became appealing because it could potentially explain the puzzling broad inclination distribution of the jovian Trojans. Motivated by this possibility, we proceeded with a far more comprehensive, and time consuming, set of simulations of this idea.

The first step in this expanded study was to determine exactly when the Trojans become unstable during the resonant crossing. For this purpose, we started by adopting the migration rates from one of the simulations reported in ref. 13. In particular, we chose a simulation where the planets migrated relatively slowly. From that simulation we measured the ratio P_S/P_J at 40 timesteps (Fig. 1a). Then, we performed 40 orbital integrations of massless test particles under the influence of the Sun, Jupiter and Saturn. The planets were placed on non-migrating orbits, with the same values of P_S/P_J as measured in Fig. 1a. The initial distribution of test particles was chosen to mimic the current distribution of Trojans relative to Jupiter. Each simulation covered 2×10^5 yr, and the fraction of the initial test particle population that remained in the Trojan region is reported in Fig. 1b, where each simulation is represented by a single point. We note two planetary configurations that are critical for the survivability of the Trojans. One occurs when $P_S/P_J \approx 2.05$ (time $t = 4.5 \times 10^5$ yr in the reference simulation), at which point all resident Trojans escape. This indicates that the entire co-orbital region is particularly unstable at this time. This instability is due to a secondary 3:1 resonance¹⁷ between $(1/P_J - 2/P_S)$ and the oscillation frequency of the Trojans around the Lagrange point. The other critical configuration occurs when $P_S/P_J \approx 2.08$ ($t = 10^6$ yr), which corresponds to a secondary 2:1 resonance between the same two frequencies, and depletes 70% of the Trojans.

In our scheme, the capture of jovian Trojans had to have occurred during these two critical planetary configurations. Thus, we designed a pair of simulations intended to study the capture process. In the first of these simulations (referred to as the slow simulation hereafter), we adopted the same migration rate as in the last paragraph. Jupiter and Saturn were forced to migrate by including a suitably chosen drag term in the planets' equations of motion, as prescribed in ref. 10, so that they reproduced the evolution of P_S/P_J shown in Fig. 1a. From 3.5×10^5 yr (just before the first critical configuration is reached) to 1.2×10^6 yr (just after the second critical configuration has passed), we supplied a steady flux of 5,466,000 planetesimals through the Jupiter-Saturn system (see Methods). This simulation

¹Observatoire de la Côte d'Azur, BP 4229, 06304 Nice Cedex 4, France. ²Department of Space Studies, Southwest Research Institute, 1050 Walnut Street, Suite 400, Boulder, Colorado 80302, USA. ³GEA/OV/UFRJ and ON/MCT, Ladeira do Pedro Antonio, 43-Centro 20.080-090, Rio de Janeiro, RJ, Brazil.

covered 10 Myr, at which point the orbits of the planets were sufficiently close to their observed ones. The second simulation was identical to the first, but with a migration rate that was three times larger and an integration time three times shorter. We will refer hereafter to this as the fast simulation. Comparably fast migration rates have been observed in many of the runs in ref. 13.

At the end of the slow simulation, 2.4×10^{-6} of the planetesimals were found to be on orbits trapped in the Trojan region. The capture efficiency rises to 1.8×10^{-5} in the fast simulation. Of these trapped Trojans, $\sim 50\%$ (the same ratio in both simulations) have libration amplitudes (the semi-amplitude of the oscillation of the angular distance from Jupiter) smaller than 30° , like 87% of the known Trojans. The vast majority of the captured Trojans with larger amplitudes of libration would not survive up to current times, because their dynamics are unstable on long timescales¹⁸. Thus, we restrict the analysis of our fictitious Trojans to those objects with libration amplitudes less than 30° .

In terms of total mass (see Methods for a description of the mass estimates), our trapped Trojan population is quite consistent with the real population, when scaled to the mass required to move the planets the required distance. Our slow simulation predicts a total Trojan mass of $\sim 4 \times 10^{-6} M_E$ (where M_E is the Earth's mass), where the fast simulation predicts a mass of $\sim 3 \times 10^{-5} M_E$. Using the most up-to-date observations, we estimate the mass of the Trojan population with $D < 30^\circ$ to be $1.1 \times 10^{-5} M_E$. So, the actual mass of the Trojans appears to be in the range predicted by our two simulations.

The reason why the mass trapped in the Trojan region increases so sharply with the planetary migration rate is twofold. First, a faster migration rate corresponds to a proportionally higher mass flux. Thus, the transient population that resides in the co-orbital region

when this region is chaotic is proportionally enhanced. This explains a factor of about three between the results of the two simulations. Second, faster migration results in a sharper transition from instability to stability in the co-orbital region, which increases the fraction of the transient population that becomes permanently trapped. This probably explains the remaining factor of $\sim 7/3$ between the results of the two simulations.

Figure 2 shows the distribution of the captured Trojans in the space of the three fundamental orbital parameters that characterize co-orbital dynamics: the proper eccentricity e , inclination i and libration amplitude D . ('Proper' refers to parameters that are suitably averaged over short periods of time and is usually introduced to characterize oscillating orbits¹⁹.) Their computation is explained in Methods. Because the distribution of the captured objects is similar in both simulations, we have included both data sets in Fig. 2 in order to improve statistics. The distribution of the known Trojans is also plotted, for visual comparison. There is an excellent qualitative agreement between the observed and simulated distributions. The captured Trojans cover the same range of values of the orbital parameters as the observed ones. There is no macroscopic region of orbital parameter space that is both occupied by the real Trojans and is left empty by the simulated ones. In particular, simulated Trojans are found even on orbits with $D < 5^\circ$. These orbits are the hardest to populate, in any capture model⁸. We stress that the inclinations of the trapped Trojans range from 0° to 40° , like those of the observed population.

We note that our results may provide an explanation for why jovian Trojans look so similar to cometary nuclei and to some (the bluest) Centaurs and Kuiper belt objects at visible wavelengths^{20,21}. In fact, it has been argued that both the Kuiper belt^{22,23} and the scattered disk²⁴—which is the current source of Centaurs and Jupiter-family comets, and probably also the progenitor of the Oort cloud—

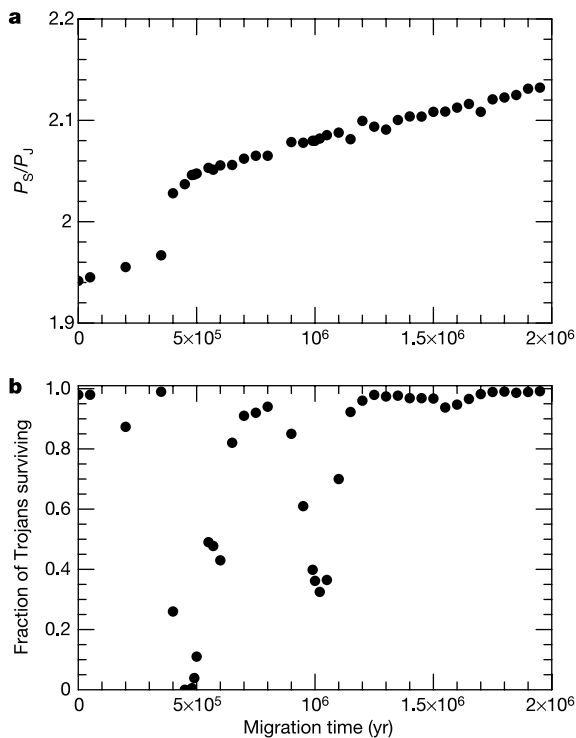


Figure 1 | The stability of Trojans during planetary migration. **a**, The temporal evolution of the ratio of orbital periods of Saturn and Jupiter (P_S and P_J , respectively) from the migration simulation that we chose from ref. 13. The magnitude of the jump in P_S/P_J when the planets cross $P_S/P_J = 2$ reflects the width of the 1:2 MMR. The planets are not captured into resonance but jump over it. **b**, The fraction of the Trojan population that survives for 2×10^5 yr in the co-orbital region, as a function of P_S/P_J (and hence of migration time).

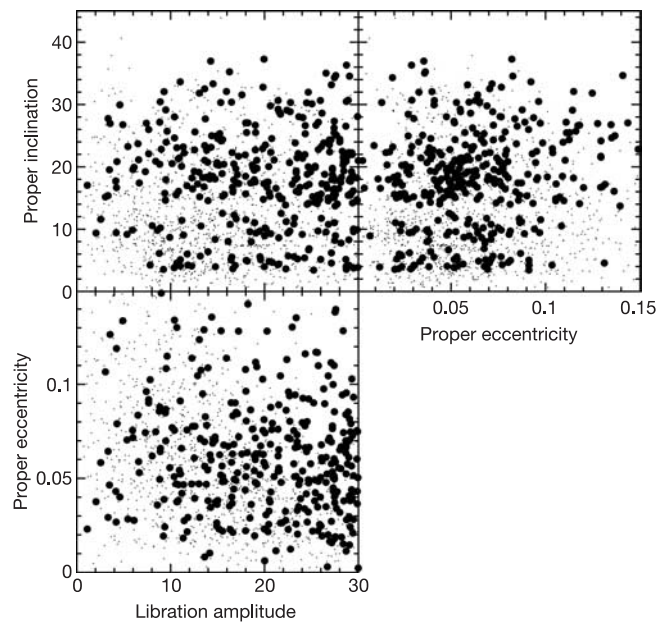


Figure 2 | Comparison of the orbital distribution of Trojans between model and observations. The simulation results are shown as filled circles and the observations as dots in the space of the three orbital parameters for co-orbital motion. The distribution of the simulated Trojans is somewhat skewed towards large libration amplitudes, relative to the observed population. However, this is not a serious problem because a fraction of the planetesimals with the largest amplitudes would leave the Trojan region during the subsequent 4 Gyr of evolution¹⁸, leading to a better match. The similarity between the two inclination distributions is strong support for our model. Libration amplitude and proper inclination are measured in degrees.

originated in the planetesimal disk that drove planetary migration. Our model places the origin of jovian Trojans in the same parent population.

Our results may also prove an explanation for the fact that Trojans are apparently deficient in water and organics²⁵. Before being captured in the Trojan region, planetesimals typically evolved through a large eccentricity phase that brought them relatively close to the Sun. Indeed, all the particles that spent more than 100 yr in the Trojan region in our first simulation reached a perihelion distance q of less than ~ 3 AU. Of them, 72% spent more than 10,000 yr on orbits with $q < 3$ AU, and 68% even reached $q < 2$ AU. Because it takes roughly 10,000 yr for an active Jupiter-family comet to become dormant²⁶, it is possible that the surfaces of the Trojans could have been devolatilized during their high eccentricity phase.

Our simulation shows that objects captured into Jupiter's co-orbital regions immediately after Jupiter and Saturn crossed the 1:2 MMR have an orbital distribution remarkably similar to that of the observed Trojans. In addition, it shows that the capture efficiency can explain the total number of objects observed. As our model is the only one available that can explain these features, we believe that the Trojans represent observational evidence for this resonance crossing, which has also been shown elsewhere¹³ to produce the correct planetary orbits. Thus, this work, together with refs 13 and 14, provides a self-consistent view of the formation and primordial evolution of the Solar System.

METHODS

Simulation of Trojan capture. We start with our 'slow' simulation, where Jupiter and Saturn are forced to migrate as in Fig. 1a. The flux of planetesimals is modelled by setting test particles on Saturn crossing orbits with orbital periods larger than P_S and a distribution of eccentricities and inclinations that mimic that in our reference simulation from ref. 13 when the 1:2 MMR is crossed. Every time that a test particle is dynamically eliminated, it is reintroduced on its original trans-saturnian orbit rescaled to the current position of Saturn. In this way, the number of particles in the simulation at any time is constant (1,163,000) and their orbital distribution remains in steady state. In total, 5,466,000 particles are eliminated and reintroduced during the considered time-span. At $t = 1.2 \times 10^6$ yr, when the co-orbital region becomes stable again, 98 particles are found on Trojan-like orbits. These particles are each cloned 19 times. The integration is then continued with the planets migrating, for 10 Myr, until the planets come reasonably close to their current semimajor axes. A drag force is also added to the planets' equations of motion, in order to slowly damp their eccentricities to their current values. At the end of the simulation, 266 particles are in the Trojan region. The final trapping efficiency is $266/20/5,466,000 \approx 2.4 \times 10^{-6}$.

In the 'fast' simulation, the migration rate of the planets is increased by a factor of three. A total of 2,773,000 particles are eliminated and reintroduced. 174 particles are found to be on Trojan-like orbits at the end of the second 'critical planetary configuration'. Of these particles, cloned 9 times each, 486 survive in the Trojan region at the end of planetary migration. The final trapping efficiency is $486/10/2,773,000 \approx 1.8 \times 10^{-5}$.

The above simulations did not take into account Uranus and Neptune. These planets could affect the capture of Trojans in two ways. Immediately after the 1:2 MMR crossing they provided kicks to Saturn during close encounters. Thus, we modify the first stage of the above simulations by including stochastic kicks to Saturn every 150,000 years with a magnitude of 0.53 km s^{-1} (based on ref. 13). Then during the post-capture, 10 Myr migration, Uranus and Neptune could destabilize the Trojans by generating additional resonances. Thus, we perform again the second stage simulation, but including Uranus and Neptune. These planets are forced to migrate from 16.5 and 20 AU to their current positions, while their eccentricities are damped from 0.1. We find that the inclusion of the ice giants does not affect Trojan capture.

Estimates of Trojan mass. According to ref. 13, $\sim 3.4 M_E$ of planetesimals are cycled through the system as the planets migrate through the unstable Trojan configurations. Of the trapped planetesimals, $\sim 50\%$ are in the region $D < 30^\circ$. The mass of captured Trojans is the product of $3.4 M_E$, 0.5, and the capture efficiency of the corresponding simulation.

According to ref. 27, the current mass of the Trojans is ~ 3 – 25 times larger than the value we find. However, ref. 27 probably overestimated the real value because it assumed: (1) an outdated density of 2 g cm^{-3} , whereas it is now

believed to be $\rho = 1.3 \text{ g cm}^{-3}$ (refs 28, 29); (2) an outdated mean albedo $p_v = 0.04$, whereas later observations²⁰ showed that it is probably $p_v = 0.056$, and (3) an absolute magnitude (H) distribution that predicts 2.5 times more objects with $H < 11$ than observed.

Correcting for (1) and (2), while keeping the H -distribution shown in Fig. 9 of ref. 2 reduces the Trojan mass estimate to $2.5 \times 10^{-5} M_E$. Correcting for (3) requires a more involved procedure. Reference 27 constrains the slope of the H -distribution for $H > 10.5$, but their estimate of the total number is problematic because of the paucity of bright objects observed in their narrow field deep survey. To overcome this problem, we use the most recent catalogue of Trojan bodies (<http://Hamilton.unipi.it/cgi-bin/astdys/astibo>) which, according to SDSS findings (Gy. M. Svabo and Z. Ivezić, personal communication) is complete up to $H = 11.5$. Beyond this threshold we extrapolate the catalogue's distribution using the slope given in ref. 27. This reduces the total mass of the Trojans to $1.3 \times 10^{-5} M_E$, 87% of which is in the considered $D < 30^\circ$ region.

Computation of Trojan proper elements. We integrate each Trojan orbit for 10^5 yr under the gravitational influence of only the Sun and Jupiter. No planetary migration is imposed. The numerical output is digitally filtered³⁰ in order to eliminate the short periodic oscillations of the orbital elements. The libration amplitude D is computed as $(\delta\lambda_{\max} - \delta\lambda_{\min})/2$, where $\delta\lambda$ is the difference between the mean longitude of the Trojan and of Jupiter, and the suffices min and max denote, respectively, its minimal and maximal value over a libration cycle. The proper eccentricity is computed as $(k_{\max} - k_{\min})/2$, where $k = e \sin \varpi$, ϖ is the Trojan's perihelion longitude and $k_{\max/\min}$ are computed over a secular oscillation of the Trojan's orbit. The proper inclination is computed in a similar way. This procedure is consistent with that used in ref. 19 for the real Trojans, which allows a direct comparison in Fig. 2.

Received 6 December 2004; accepted 11 March 2005.

- Marzari, F. & Scholl, H. Capture of Trojans by a growing proto-Jupiter. *Icarus* **131**, 41–51 (1998).
- Fleming, H. J. & Hamilton, D. P. On the origin of the Trojan asteroids: Effects of Jupiter's mass accretion and radial migration. *Icarus* **148**, 479–493 (2000).
- Yoder, C. F. Notes on the origin of the Trojan asteroids. *Icarus* **40**, 341–344 (1979).
- Peale, S. J. The effect of the nebula on the Trojan precursors. *Icarus* **106**, 308–322 (1993).
- Kary, D. M. & Lissauer, J. J. Nebular gas drag and planetary accretion. II. Planet on an eccentric orbit. *Icarus* **117**, 1–24 (1995).
- Kortenkamp, S. J. & Hamilton, D. P. Capture of Trojan asteroids in the early Solar Nebula. *Bull. Am. Astron. Soc.* **33**, 1086 (2001).
- Shoemaker, E. M., Shoemaker, C. S. & Wolfe, R. F. in *Asteroids II* (eds Binzel, R. P., Gehrels, T. & Matthews, M. S.) 487–523 (Univ. Arizona Press, Tucson, 1989).
- Marzari, F., Scholl, H., Murray, C. & Lagerkvist, C. in *Asteroids III* (eds Bottke, W. F., Cellino, A., Paolicchi, P. & Binzel, R. P.) 725–738 (Univ. Arizona Press, Tucson, 2002).
- Fernandez, J. A. & Ip, W. H. Some dynamical aspects of the accretion of Uranus and Neptune—The exchange of orbital angular momentum with planetesimals. *Icarus* **58**, 109–120 (1984).
- Malhotra, R. The origin of Pluto's peculiar orbit. *Nature* **365**, 819–821 (1993).
- Hahn, J. M. & Malhotra, R. Orbital evolution of planets embedded in a planetesimal disk. *Astron. J.* **117**, 3041–3053 (1999).
- Gomes, R. S., Morbidelli, A. & Levison, H. F. Planetary migration in a planetesimal disk: why did Neptune stop at 30 AU? *Icarus* **170**, 492–507 (2004).
- Tsiganis, K., Gomes, R., Morbidelli, A. & Levison, H. F. Origin of the orbital architecture of the giant planets of the Solar System. *Nature* doi:10.1038/nature03539 (this issue).
- Gomes, R., Tsiganis, K., Morbidelli, A. & Levison, H. F. Origin of the cataclysmic Late Heavy Bombardment period of the terrestrial planets. *Nature* doi:10.1038/nature03676 (this issue).
- Gomes, R. S. Dynamical effects of planetary migration on primordial Trojan-type asteroids. *Astron. J.* **116**, 2590–2597 (1998).
- Michtchenko, T. A., Beaugé, C. & Roig, F. Planetary migration and the effects of mean motion resonances on Jupiter's Trojan asteroids. *Astron. J.* **122**, 3485–3491 (2001).
- Kortenkamp, S. J., Malhotra, R. & Michtchenko, T. Survival of Trojan-type companions of Neptune during primordial planet migration. *Icarus* **167**, 347–359 (2004).
- Levison, H. F., Shoemaker, E. M. & Shoemaker, C. S. Dynamical evolution of Jupiter's Trojan asteroids. *Nature* **385**, 42–44 (1997).
- Milani, A. The Trojan asteroid belt: Proper elements, stability, chaos and families. *Celest. Mech. Dyn. Astron.* **57**, 59–94 (1993).
- Fernández, Y. R., Sheppard, S. S. & Jewitt, D. C. The albedo distribution of Jovian Trojan asteroids. *Astron. J.* **126**, 1563–1574 (2003).
- Barucci, M. A., Cruikshank, D. P., Mottola, S. & Lazzarin, M. in *Asteroids III*

- (eds Bottke, W. F., Cellino, A., Paolicchi, P. & Binzel, R. P.) 273–288 (Univ. Arizona Press, Tucson, 2002).
22. Gomes, R. S. The origin of the Kuiper Belt high-inclination population. *Icarus* **161**, 404–418 (2003).
 23. Levison, H. F. & Morbidelli, A. The formation of the Kuiper belt by the outward transport of bodies during Neptune's migration. *Nature* **426**, 419–421 (2003).
 24. Duncan, M. J. & Levison, H. F. A scattered comet disk and the origin of Jupiter family comets. *Science* **276**, 1670–1672 (1997).
 25. Emery, J. P. & Brown, R. H. The surface composition of Trojan asteroids: constraints set by scattering theory. *Icarus* **170**, 131–152 (2004).
 26. Levison, H. F. & Duncan, M. J. From the Kuiper Belt to Jupiter-family comets: The spatial distribution of ecliptic comets. *Icarus* **127**, 13–32 (1997).
 27. Jewitt, D. C., Trujillo, C. A. & Luu, J. X. Population and size distribution of small Jovian Trojan asteroids. *Astron. J.* **120**, 1140–1147 (2000).
 28. Merline, W. J. *et al.* in *Asteroids III* (eds Bottke, W. F., Cellino, A., Paolicchi, P. & Binzel, R. P.) 289–314 (Univ. Arizona Press, Tucson, 2002).
 29. Britt, D. T., Yeomans, D., Housen, K. & Consolmagno, G. in *Asteroids III* (eds Bottke, W. F., Cellino, A., Paolicchi, P. & Binzel, R. P.) 485–500 (Univ. Arizona Press, Tucson, 2002).
 30. Quinn, T. R., Tremaine, S. & Duncan, M. A three million year integration of the earth's orbit. *Astron. J.* **101**, 2287–2305 (1991).

Acknowledgements R.G. is grateful to the Conselho Nacional de Desenvolvimento Científico e Tecnológico for financial support of his sabbatical year in the OCA observatory in Nice. The work of K.T. was supported by an EC Marie Curie Individual Fellowship. A.M. and H.F.L. thank the CNRS and the NSF for funding the collaboration between the OCA and the SWRI groups. H.F.L. is grateful to NASA's Origins and PG&G programmes.

Author Information Reprints and permissions information is available at npg.nature.com/reprintsandpermissions. The authors declare no competing financial interests. Correspondence and requests for materials should be addressed to A.M. (morby@obs-nice.fr).

LETTERS

Origin of the cataclysmic Late Heavy Bombardment period of the terrestrial planets

R. Gomes^{1,2}, H. F. Levison^{2,3}, K. Tsiganis² & A. Morbidelli²

The petrology record on the Moon suggests that a cataclysmic spike in the cratering rate occurred ~700 million years after the planets formed¹; this event is known as the Late Heavy Bombardment (LHB). Planetary formation theories cannot naturally account for an intense period of planetesimal bombardment so late in Solar System history². Several models have been proposed to explain a late impact spike^{3–6}, but none of them has been set within a self-consistent framework of Solar System evolution. Here we propose that the LHB was triggered by the rapid migration of the giant planets, which occurred after a long quiescent period. During this burst of migration, the planetesimal disk outside the orbits of the planets was destabilized, causing a sudden massive delivery of planetesimals to the inner Solar System. The asteroid belt was also strongly perturbed, with these objects supplying a significant fraction of the LHB impactors in accordance with recent geochemical evidence^{7,8}. Our model not only naturally explains the LHB, but also reproduces the observational constraints of the outer Solar System⁹.

Previous work⁹ explains the current orbital architecture of the planetary system by invoking an initially compact configuration in which Saturn's orbital period was less than twice that of Jupiter. After the dissipation of the gaseous circumsolar nebula, Jupiter's and Saturn's orbits diverged as a result of their interaction with a massive disk of planetesimals, and thus the ratio of their orbital periods, P_S/P_J , increased. When the two planets crossed their mutual 1:2 mean motion resonance (1:2 MMR, that is, $P_S/P_J = 2$) their orbits became eccentric. This abrupt transition temporarily destabilized the giant planets, leading to a short phase of close encounters among Saturn, Uranus and Neptune. As a result of these encounters, and of the interactions of the ice giants with the disk, Uranus and Neptune reached their current heliocentric distances and Jupiter and Saturn evolved to their current orbital eccentricities⁹. The main idea of this Letter is that the same planetary evolution could explain the LHB, provided that Jupiter and Saturn crossed the 1:2 MMR roughly 700 Myr after they formed. Thus, our goal is to determine if there is a generic mechanism that could delay the migration process.

In previous studies^{9–12}, planet migration started immediately because planetesimals were placed close enough to the planets to be violently unstable. Although this type of initial condition was reasonable for the goals of those studies, it is unlikely. Planetesimal-driven migration is probably not important for planet dynamics as long as the gaseous massive solar nebula exists. The initial conditions for the migration simulations should represent the system that existed at the time the nebula dissipated. Thus, the planetesimal disk should contain only those particles that had dynamical lifetimes longer than the lifetime of the solar nebula. In planetary systems like those we adopt from ref. 9, we find that they had to be beyond ~15.3 AU (Fig. 1), leading to the initial conditions illustrated in Fig. 2a.

In this configuration, the initial speed of migration would be

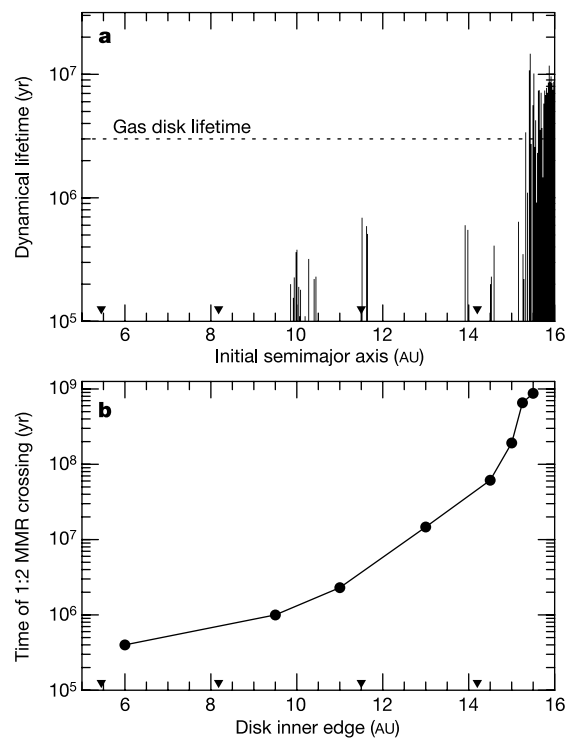


Figure 1 | Disk location and LHB timing. **a**, The histogram reports the average dynamical lifetime of massless test particles placed in a planetary system (shown as triangles) with Jupiter, Saturn and the ice giants on nearly circular, co-planar orbits at 5.45, 8.18, 11.5 and 14.2 AU, respectively. Initially, we placed 10 particles with $e = i = 0$ (where e is eccentricity and i is inclination) and random mean anomaly at each semimajor axis. Stable Trojans of the planets have been removed from this computation. Each vertical bar in the plot represents the average lifetime for those 10 particles. We define ‘dynamical lifetime’ as the time required for a particle to encounter a planet within a Hill radius. A comparison between the histogram and the putative lifetime of the gaseous nebula²⁰ argues that, when the latter dissipated, the inner edge of the planetesimal disk had to be about 1–1.5 AU beyond the outermost ice giant. **b**, Time at which Jupiter and Saturn crossed the 1:2 MMR, as a function of the location of the planetesimal disk's inner edge, as determined from our first set of migration simulations. In all cases, the disk had a surface density equivalent to $1.9 M_E$ per 1 AU annulus. The outer edge of the disk was varied so that the total mass of the disk was $35 M_E$. The disk was initially very dynamically cold, with $e = 0$ and $i < 0.5^\circ$. A comparison between **a** and **b** shows that a disk that naturally should exist when the nebula dissipated would produce a 1:2 MMR crossing at a time comparable to that of the LHB event.

¹ON/MCT and GEA/OV/UFRJ, Ladeira do Pedro Antonio, 43 Centro 20.080-090, Rio de Janeiro, RJ, Brazil. ²Observatoire de la Côte d'Azur, CNRS, BP 4229, 06304 Nice Cedex 4, France. ³Department of Space Studies, Southwest Research Institute, 1050 Walnut Street, Suite 400, Boulder, Colorado, USA.

dependent on the rate at which disk particles evolve onto planet-crossing orbits. The time at which Jupiter and Saturn cross their 1:2 MMR depends on: (1) their initial distance from the location of the resonance, (2) the surface density of the disk near its inner edge, and (3) the relative location of the inner edge of the disk and the outer ice giant. On the basis of the above arguments, we initially performed a series of eight simulations where the location of the inner edge of the disk was set as the unique free parameter (Fig. 1). As expected, we found a strong correlation between the location of the inner edge and the time of the 1:2 MMR crossing. For disks with inner edges near 15.3 AU (see above), we find crossing times between 192 Myr and 880 Myr (since the beginning of the simulation).

We also performed eight simulations where we varied the initial location of the ice giants by ~ 1 AU, Saturn's location by ~ 0.1 AU, the total mass of the disk by 5 Earth masses ($5M_E$), and its initial dynamical state by pushing the particles' eccentricities up to 0.1 and inclinations up to 3.5° . We found that we can delay the resonant crossing to 1.1 Gyr since the beginning of the simulation, although longer times are clearly possible for more extreme initial conditions. Therefore, we can conclude that the global instability caused by the 1:2 MMR crossing of Jupiter and Saturn could be responsible for the LHB, because the estimated date of the LHB falls in the range of the times that we found.

Figures 2 and 3 show the evolution of one of our runs from the first series of eight. Initially, the giant planets migrated slowly owing to leakage of particles from the disk (Fig. 3a). This phase lasted 880 Myr, at which point Jupiter and Saturn crossed the 1:2 MMR. After the

resonance crossing event, the orbits of the ice giants became unstable and they were scattered into the disk by Saturn. They disrupted the disk and scattered objects all over the Solar System, including the inner regions. The solid curve in Fig. 3b shows the amount of material that struck the Moon as a function of time. A total of 9×10^{21} g struck the Moon after resonance crossing—roughly 50% of this material arrived in the first 3.7 Myr and 90% arrived before 29 Myr. The total mass is consistent with the estimate⁴ of 6×10^{21} g, which was determined from the number and size distribution of lunar basins that formed around the time of the LHB epoch¹. Such an influx spike happened in all our runs. The amount of cometary material delivered to the Earth is $\sim 1.8 \times 10^{23}$ g, which is about 6% of the current ocean mass. This is consistent with upper bounds on the cometary contribution to the Earth's water budget, based on D/H ratio measurement¹³. The average amount of material accreted by the Moon during this spike was $(8.4 \pm 0.3) \times 10^{21}$ g.

The above mass delivery estimate corresponds only to the cometary contribution to the LHB, as the projectiles originated from the external massive, presumably icy, disk. However, our scheme probably also produced an influx of material from the asteroid belt. As Jupiter and Saturn moved from 1:2 MMR towards their current positions, secular resonances (which occur when the orbit of an asteroid processes at the same rate as a planet) swept across the entire belt¹⁴. These resonances can drive asteroids onto orbit with eccentricities and inclinations large enough to allow them to evolve into the inner Solar System and hit the Moon⁴.

We investigated the role of asteroid impactors in our LHB model

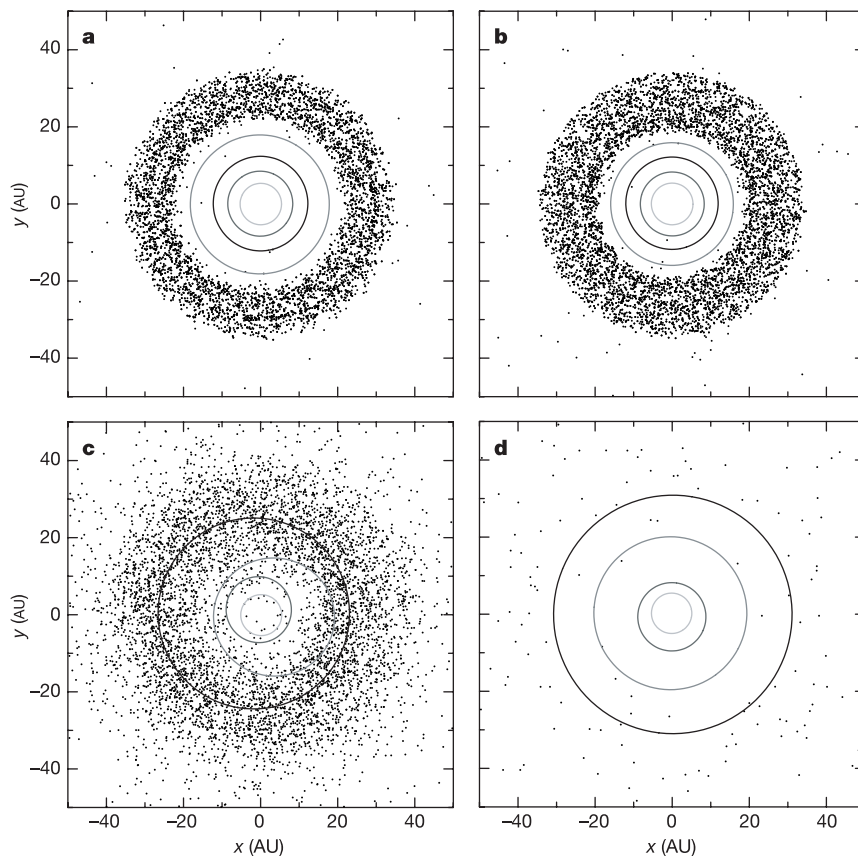


Figure 2 | The planetary orbits and the positions of the disk particles, projected on the initial mean orbital plane. The four panels correspond to four different snapshots taken from our reference simulation. In this run, the four giant planets were initially on nearly circular, co-planar orbits with semimajor axes of 5.45, 8.18, 11.5 and 14.2 AU. The dynamically cold planetesimal disk was $35M_E$, with an inner edge at 15.5 AU and an outer edge

at 34 AU. Each panel represents the state of the planetary system at four different epochs: **a**, the beginning of planetary migration (100 Myr); **b**, just before the beginning of LHB (879 Myr); **c**, just after the LHB has started (882 Myr); and **d**, 200 Myr later, when only 3% of the initial mass of the disk is left and the planets have achieved their final orbits.

by the following numerical integrations. The orbits of an asteroid belt, composed of 1,000 massless particles with semimajor axes between 2.0 and 3.5 AU, were integrated under the gravitational influence of the Sun, Venus, Earth, Mars, Jupiter and Saturn. Because formation models^{15,16} predict that the asteroid belt was partially depleted and dynamically excited well before the LHB, we set the particles' eccentricities between 0 and 0.3 and inclinations between 0° and 30°, but kept the perihelion distances, q , >1.8 AU and aphelion distances, Q , <4 AU. Jupiter and Saturn were forced to migrate at rates that varied from run to run (adopted from ref. 9) by adding a suitably chosen drag-force term to their equations of motion.

We find that objects that reach Earth-crossing orbits follow one of two general paths. Some, referred to as class 1 particles, get trapped in

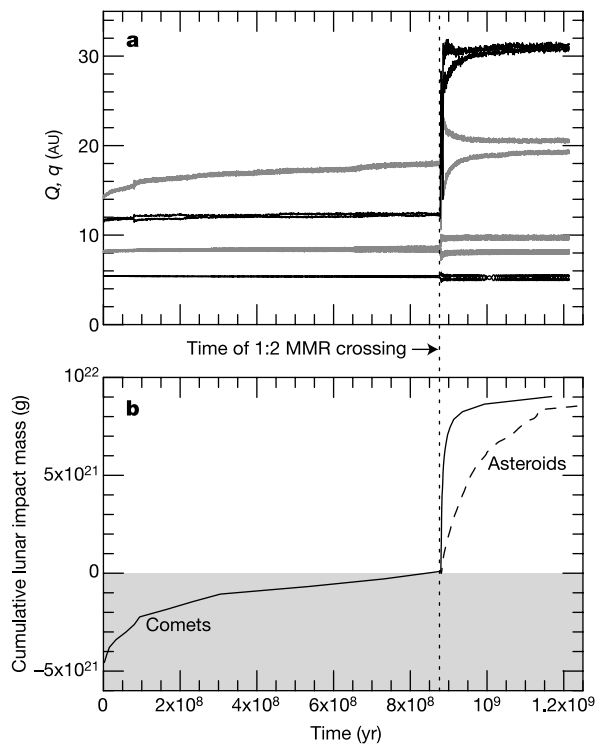


Figure 3 | Planetary migration and the associated mass flux towards the inner Solar System from a representative simulation. **a**, The evolution of the four giant planets. Each planet is represented by a pair of curves—the top and bottom curves are the aphelion and perihelion distances, Q and q , respectively. Jupiter and Saturn cross the 1:2 MMR at 880 Myr. The subsequent interaction between the planets and the disk led to the current planetary configuration as shown in ref. 9. **b**, The cumulative mass of comets (solid curve) and asteroids (dashed curve) accreted by the Moon. We have offset the comet curve so that the value is zero at the time of 1:2 MMR crossing. Thus, $\sim 5 \times 10^{21}$ g of comets was accreted before resonant crossing and 9×10^{21} g of cometary material would have struck the Moon during the LHB. Although the terrestrial planets were not included in our cometary simulations, we estimated the amount of material accreted by the Moon directly from the mass of the planetesimal disk by combining the particles' dynamical evolution with the analytic expressions in ref. 21. The impact velocity of these objects ranged from 10 to 36 km s⁻¹ with an average of 21 km s⁻¹. Estimating the asteroidal flux first requires a determination of the mass of the asteroid belt before resonant crossing. This value was determined by first combining the percentage of asteroids remaining in the belt at the end of a simulation ($\sim 10\%$, very sensitive to planet migration rate and initial asteroid distribution) with estimates of the current mass of the belt to determine the initial asteroid belt mass ($\sim 5 \times 10^{-3} M_E$). The flux was then again determined by combining the particles' dynamical evolution with the analytic expressions in ref. 21. The dashed curve shows a simulation where class 2 particles dominate. The average asteroidal impact velocity is 25 km s⁻¹.

the periape secular resonance with Saturn (which affects eccentricities) and are driven directly onto Earth-crossing orbits. Other particles, referred to as class 2, stay in the asteroid belt, but are dynamically excited by resonant sweeping onto unstable orbits. These objects slowly leak out of the asteroid belt and can evolve into the inner Solar System. The two classes produce impact spikes with different temporal behaviours. Roughly 50% of class 1 particles arrive in the first 10 Myr, while 90% arrive within ~ 30 Myr. Conversely, the median arrival time for class 2 particles is ~ 50 Myr and 90% arrive within ~ 150 Myr. Class 2 particles dominated in our runs (Fig. 3). However, a preliminary investigation into this issue shows that this result is probably sensitive to the exact evolution of the giant planets and the dynamical state of the asteroid belt. Thus, the best we can conclude is that the impact spike due to asteroids is between these two extremes.

We find that $(3-8) \times 10^{21}$ g of asteroids hit the Moon during our simulations (Fig. 3). This amount is comparable to the amount of comets. So, our model predicts that the LHB impactors should have been a mixture of comets and asteroids. Unfortunately, we cannot say with any certainty the exact ratio of comets to asteroids in our model because, although the amount of cometary material is fairly well constrained (probably better than a factor of 2), the amount of asteroidal material is not well known (and could be outside the range reported above), because we do not have good estimates of the mass distribution in the asteroid belt before the LHB. It should also be noted that this ratio is probably a function of impactor size, because comets and asteroids probably have different size distributions. This ratio probably also varied with time. Within the first ~ 30 Myr comets dominated according to these simulations, but the last impactors were asteroidal. This is consistent with recent cosmochemical findings suggesting that some of the Moon's basins were formed by asteroids^{7,8}.

Our results support a cataclysmic model for the lunar LHB. Although many aspects of the LHB are not well known¹, our simulations reproduce two of the main characteristics attributed to this episode: (1) the 700 Myr delay between the LHB and terrestrial planet formation, and (2) the overall intensity of lunar impacts. Our model predicts a sharp increase in the impact rate at the beginning of the LHB. Unfortunately, the available lunar data are not yet capable of addressing this prediction.

Our model also has the advantage of supplying impactors that are a mixture of comets and asteroids. Our model predicts that the asteroid belt was depleted by a factor of ~ 10 during the LHB. This depletion does not contradict collisional evolution models^{17,18}. On the contrary, the late secular resonance sweeping could explain why we do not see a large number of asteroid families that were produced during the LHB¹⁹. Our model predicts that the LHB lasted from between ~ 10 Myr and ~ 150 Myr. Correspondingly, the drop-off in impact rates could be quite fast (with 50% of the impacts occurring in the first 3.7 Myr and 90% in 29 Myr) or moderately slow (with 50% of the impacts occurring in the first 50 Myr and 90% in 150 Myr). We are unable to pinpoint more exact values because the duration and the drop-off of the LHB depends on the relative contributions of class 1 asteroids, class 2 asteroids, and comets, which in turn are very sensitive to the pre-LHB orbital structure of the asteroid belt.

Most importantly, our scheme for the LHB is the result of a generic migration-delaying mechanism, followed by an instability, which is itself induced by a deterministic mechanism of orbital excitation of the planets⁹. This revised planetary migration scheme naturally accounts for the currently observed planetary orbits⁹, the LHB, the present orbital distribution of the main-belt asteroids and the origin of Jupiter's Trojans¹⁹.

Received 6 December 2004; accepted 18 April 2005.

- Hartmann, W. K., Ryder, G., Dones, L. & Grinspoon, D. in *Origin of the Earth and Moon* (eds Canup, R. & Righter, K.) 493–512 (Univ. Arizona Press, Tucson, 2000).

2. Morbidelli, A., Petit, J.-M., Gladman, B. & Chambers, J. A plausible cause of the Late Heavy Bombardment. *Meteorit. Planet. Sci.* **36**, 371–380 (2001).
3. Zappala, V., Cellino, A., Gladman, B. J., Manley, S. & Migliorini, F. Asteroid showers on Earth after family break-up events. *Icarus* **134**, 176–179 (1998).
4. Levison, H. F. *et al.* Could the lunar “Late Heavy Bombardment” have been triggered by the formation of Uranus and Neptune? *Icarus* **151**, 286–306 (2001).
5. Chambers, J. E. & Lissauer, J. J. A new dynamical model for the lunar Late Heavy Bombardment. *Lunar Planet. Sci. Conf. XXXIII*, abstr. 1093 (2002).
6. Levison, H. F., Thommes, E. W., Duncan, M. J., Dones, L. A. in *Debris Disks and the Formation of Planets: A Symposium in Memory of Fred Gillett (11–13 April 2002, Tucson, Arizona)* (eds Caroff, L., Moon, L. J., Backman, D. & Praton, E.) 152–167 (ASP Conf. Ser. 324, Astronomical Society of the Pacific, San Francisco, 2005).
7. Kring, D. A. & Cohen, B. A. Cataclysmic bombardment throughout the inner Solar System 3.9–4.0 Ga. *J. Geophys. Res. Planets* **107**(E2), 4–10 (2002).
8. Tagle, R. LL-ordinary chondrite impact on the Moon: Results from the 3.9 Ga impact melt at the landing site of Apollo 17. *Lunar Planet. Sci. Conf. XXXVI*, abstr. 2008 (2005).
9. Tsiganis, K., Gomes, R., Morbidelli, A. & Levison, H. F. Origin of the orbital architecture of the giant planets of the Solar System. *Nature* doi:10.1038/nature03539 (this issue).
10. Fernandez, J. A. & Ip, W.-H. Some dynamical aspects of the accretion of Uranus and Neptune—The exchange of orbital angular momentum with planetesimals. *Icarus* **58**, 109–120 (1984).
11. Hahn, J. M. & Malhotra, R. Orbital evolution of planets embedded in a planetesimal disk. *Astron. J.* **117**, 3041–3053 (1999).
12. Gomes, R. S., Morbidelli, A. & Levison, H. F. Planetary migration in a planetesimal disk: Why did Neptune stop at 30 AU? *Icarus* **170**, 492–507 (2004).
13. Morbidelli, A. *et al.* Source regions and timescales for the delivery of water to Earth. *Meteorit. Planet. Sci.* **35**, 1309–1320 (2000).
14. Gomes, R. S. Dynamical effects of planetary migration on the primordial asteroid belt. *Astron. J.* **114**, 396–401 (1997).
15. Wetherill, G. W. An alternative model for the formation of the asteroids. *Icarus* **100**, 307–325 (1992).
16. Petit, J., Morbidelli, A. & Chambers, J. The primordial excitation and clearing of the asteroid belt. *Icarus* **153**, 338–347 (2001).
17. Davis, D. R., Ryan, E. V. & Farinella, P. Asteroid collisional evolution: results from current scaling algorithms. *Planet. Space Sci.* **42**, 599–610 (1994).
18. Bottke, W. *et al.* The fossilized size distribution of the main asteroid belt. *Icarus* **175**(1), 111–140 (2005).
19. Morbidelli, A., Levison, H. F., Tsiganis, K. & Gomes, R. Chaotic capture of Jupiter’s Trojan asteroids in the early Solar System. *Nature* doi:10.1038/nature03540 (this issue).
20. Haisch, K. E., Lada, E. A. & Lada, C. J. Disk frequencies and lifetimes in young clusters. *Astrophys. J.* **553**, L153–L156 (2001).
21. Wetherill, G. W. Collisions in the asteroid belt. *J. Geophys. Res.* **72**, 2429–2444 (1967).

Acknowledgements R.G. thanks Conselho Nacional de Desenvolvimento Científico e Tecnológico for support for his sabbatical year in the OCA observatory in Nice. K.T. was supported by an EC Marie Curie Individual Fellowship. A.M. and H.F.L. thank the CNRS and the NSF for funding collaboration between the OCA and the SWRI groups. H.F.L. was supported by NASA’s Origins and PG&G programmes.

Author Information Reprints and permissions information is available at npg.nature.com/reprintsandpermissions. The authors declare no competing financial interests. Correspondence and requests for materials should be addressed to A.M. (morby@obs-nice.fr).